# Large liquid-scintillator trackers for neutrino experiments

L. Benussi, N. Bruski, N. d'Ambrosio, Y. Déclais, J. Dupraz, J P. Fabre, V. Fanti, E. Forton, D. Frekers, A. Frenkel, et al.

EUROPEAN ORGANIZATION FOR NUCLEAR RESEARCH

CERN-EP/2002-006
14 January 2002

# Large liquid-scintillator trackers for neutrino experiments

L. Benussi [a,1], N. Bruski [b], N. D'Ambrosio [c] Y. Déclais [d], J. Dupraz [e], J.-P. Fabre [e], V. Fanti [a,2], E. Forton[f], D. Frekers [c], A. Frenkel [g], C. Girerd [d], S.V. Golovkin[h], G. Gregoire [f], K. Harrison [g], G. Jonkmans [i], P. Jonsson[d], S. Katsanevas [d], I. Kreslo [j,3], J. Marteau[d], G. Martellotti [g], S. Martinez [g], A.M. Medvedkov [h], G. Moret[d], K. Niwa[k], V. Novikov [h], G. Van Beek [a], G. Penso [g], V.G. Vasil'chenko [h], J.-L. Vuilleumier [i], G. Wilquet [a], P. Zucchelli [e]

[a] *IIHE, ULB-VUB, Bruxelles, Belgium*
[b] *Università "Federico II" and INFN, Napoli, Italy*
[c] *Westfälische Wilhelms-Universität, Münster, Germany*
[d] *Université Claude Bernard, Lyon, France*
[e] *CERN, Genève, Switzerland*
[f] *Université Catholique de Louvain, Louvain-La-Neuve, Belgium*
[g] *Università "La Sapienza" and INFN, Roma, Italy*
[h] *IHEP, Protvino, Russia*
[i] *Université de Neuchatel, Switzerland*
[j] *JINR, Dubna, Russia*
[k] *Nagoya University, Japan*

**Abstract**

Results are given on tests of large particle trackers for the detection of neutrino interactions in long-baseline experiments. Module prototypes have been assembled using $TiO_2$-doped polycarbonate panels. These were subdivided into cells of $\sim 1$ cm$^2$ cross section and 6 m length, filled with liquid scintillator. A wavelength-shifting fibre inserted in each cell captured a part of the scintillation light emitted when a cell was traversed by an ionizing particle. Two different fibre-readout systems have been tested: an optoelectronic chain comprising an image intensifier and an Electron Bombarded CCD (EBCCD); and a hybrid photodiode (HPD). New, low-cost liquid scintillators have been investigated for applications in large underground detectors. Testbeam studies have been performed using a commercially available liquid scintillator. The number of detected photoelectrons for minimum-ionizing particles crossing a module at different distances from the fibre readout end was 6 to 12 with the EBCCD chain and a mirror at the non-readout end; 4 to 10 with the HPD and no mirror. The light-attenuation lengths in the fibres were $\sim 9.4$ m with the EBCCD and $\sim 6.4$ m with the HPD. The detector response to electron showers has also been measured. After 10 radiation lengths of lead, the transverse position of the incoming electron was determined with a precision of a few millimeters for electrons of 4 GeV, and with a precision of 1.5$-$2.0 cm for electrons of 1 GeV.

*PACS:* 29.40.Mc; 29.40.Gx; 29.40.Vj
*Keywords:* Tracking and position-sensitive detectors; Scintillation detectors; Liquid scintillators; EBCCD.

*(Submitted to Nuclear Instruments & Methods A)*

[1]Now at LNF, Frascati, Italy.
[2]Now at INFN, Cagliari, Italy.
[3]Now at CERN, Genève, Switzerland.

# 1 Introduction

The question of whether neutrinos have non-vanishing mass is one of the most intriguing of particle physics. Since neutrino masses are probably too small to be measured from decay kinematics, the most promising line of investigation is to search for neutrino oscillation, a process that occurs only if the mass values, however low, are different from zero. Indications that such oscillations may occur come from observations of atmospheric neutrinos by Kamiokande [1], Soudan-2 [2], MACRO [3] and Super-Kamiokande [4], where anomalous results for $\nu_\mu$ flux and zenith-angle distribution suggest the existence of $\nu_\mu \leftrightarrow \nu_\tau$ oscillations. This possibility is to be tested using initially pure $\nu_\mu$ beams in long-baseline accelerator experiments: K2K [5] and MINOS [6] aim at observation of $\nu_\mu$ disappearance; OPERA [7], proposed by CERN and LNGS, searches for $\nu_\tau$ appearance.

The OPERA detector is conceptually similar to that of the DONUT experiment [8], which has succeeded in detecting $\nu_\tau$ interactions. It consists of a series of "walls", placed perpendicularly to the neutrino beam and obtained by piling up "bricks". Each brick contains layers of emulsion film alternating with lead plate. An electronic tracker is placed downstream of each wall and allows selection of the brick in which a neutrino interaction occurs, so guiding the emulsion scanning.

The electronic trackers for the OPERA experiment will have dimensions of about $6.7 \times 6.7$ m$^2$ and a moderate spatial resolution, of the order of a centimetre. One possibility is to use a novel type of detector, based on polycarbonate panels filled with liquid scintillator (LS), with readout via wavelength-shifting (WLS) fibres. First investigations of the basic technique were undertaken at CERN [9,10], and a structurally similar detector, but based on polyvinylchloride panels, has been studied independently for the MINOS experiment [11].

In the present paper we report on the design and test of prototype tracker modules, assembled from panels of polycarbonate doped with $TiO_2$. The panels were subdivided into cells with a cross section of the order of 1 cm$^2$ and a length of 6 m. A wavelength-shifting fibre, of $\sim 1.2$ mm diameter, was inserted in each cell, then the panels were sealed and filled with liquid scintillator. When a charged particle traversed the liquid scintillator, a part of the emitted light was absorbed in the WLS fibre, either directly or after undergoing diffuse reflections at the cell walls. Some fraction of the wavelength-shifted light was captured in the fibre and propagated to the readout end, where it could be detected by an optoelectronic device.

A first testbeam study, using a 70 GeV $\mu^-$ beam, has been performed to evaluate light yields, light-attenuation lengths in fibres, crosstalk between cells, and other technical characteristics, for six full-scale modules. Each module measured $\sim 6 \times 1$ m$^2$ and comprised 90 cells of $0.9 \times 1.1$ cm$^2$ cross section.

A second testbeam study has been performed using panels based on a polycarbonate with an increased concentration of $TiO_2$. Light yields have again been evaluated, and the effect of cell width has been investigated. To simulate the OPERA setup, six modules of surface area $6.0 \times 0.55$ m$^2$, each containing 50 cells of $0.9 \times 1.1$ cm$^2$, were tested with a variable thickness of lead (0−5.6 cm) placed in front. Measurements were made using beams of $\pi^-$ and $e^-$, with energies in the range 1−10 GeV.

# 2 Prototype detector

## 2.1 Multi-cell polycarbonate panels

The modules used for most of the tests performed consisted of cells with an inner cross section of $0.9 \times 1.1\,\mathrm{cm}^2$ and a wall thickness of 0.3 mm (Fig. 1). An investigation of the effect of cell dimensions on light-collection efficiency has been performed using a specially prepared module, comprising cells of different cross sections: $0.9{\times}1.1$ cm$^2$, $0.9{\times}2.2$ cm$^2$ and $0.9{\times}3.3$ cm$^2$.

The multi-cell panels are obtained by extrusion of polycarbonate doped with $TiO_2$. This white dopant reflects the scintillation light inside a cell, increasing the light captured by the WLS fibre and reducing optical crosstalk between neighbours. The $TiO_2$ concentration for the polycarbonate used in the first testbeam study was 8 %, for which the crosstalk on each side of a cell was at the level of 10 %. For subsequent tests, the dopant concentration was increased to 20 %, the maximum compatible with the extrusion process. This reduced the crosstalk to about 3 % and improved the light output.

The reflection characteristics of the panel material are shown in Fig. 2. They were measured with a Varian[1] Cary 5 spectrophotometer, which allowed separation of the components from specular and diffuse reflection. The diffuse component dominates, and for the wavelengths of emission of the scintillators of interest the total reflectivity is about 80 %.

A groove with a depth of several centimetres is cut in the inter-cell partitions, at the ends of each panel. This allows communication between cells during filling, achieved via the two outermost cells of a panel. Wavelength-shifting fibres are threaded through the cells, then the cells are sealed by injecting a small amount of silicone into their ends.

To allow a check of the light transmission of the fibres, with or without LS inside the cells, each panel has two electro-luminescent strips[2] glued on one side (Fig. 1), near the cell ends and perpendicular to their lengths. The panels are covered with a black plastic film. When pulsed with 40 V, the luminescent strips emit light in the wavelength interval 490-550 nm. As the cell walls are slightly translucent, the light can reach the fibres and, after wavelength shifting, be captured. In Fig. 3a we show the light recorded for each fibre in a module, following emission by the strip nearer the readout end. In Fig. 3b we show the ratio between the light recorded when the strip further from the readout end is pulsed, and that recorded when the nearer strip is pulsed. The observation of a lower value for the 15th fibre in Fig. 3a, but not in Fig. 3b, indicates that this fibre is damaged at a point outside the region between the two strips.

## 2.2 WLS fibres

The WLS fibres used were Kuraray[3] type Y11 plastic fibres, with a core of diameter 1.096 mm and refractive index 1.59; a first cladding of thickness 30 $\mu$m and refractive index 1.49; a second cladding of thickness 20 $\mu$m and refractive index 1.42. The core material of the fibres had peak absorption in the blue region, well matched with the emission spectrum of the LS tested. The light emitted after wavelength shifting had peak intensity in the green region, for which photocathodes of high quantum efficiency are available. Spectra for the light emerging from the fibres have been measured in the

[1] Varian Inc., Palo Alto, CA 94304-1038, USA.
[2] Lumitec AG, CH-9056 Gais, Switzerland
[3] Kuraray Co. Ltd., Tokyo 103-8254, Japan.

laboratory, for different distances between emission point and fibre end, and are shown in Fig. 4. Self-absorption causes the light to be more strongly attenuated at shorter wavelengths.

Fibres extended a distance of 0.5−1.5 m (depending on the readout sytem) beyond the ends of the sealed polycarbonate panels. The fibre ends were gathered together in a well-defined order and glued in an optical connector, directly coupled to the first photocathode of the readout system.

Fibres are mechanically fixed to the modules only by the silicone at the ends of each cell. Inside the cells, the positions of the fibres are unknown. The relative light-collection efficiency inside a cell uniformly crossed by ionizing particles has been evaluated for different fibre positions using a Monte-Carlo simulation, described in section 3.1. The maximum variation in light-collection efficiency between any two fibre locations is found to be less than ± 4 %, showing that the positioning of the fibres inside the cells is not critical.

## 2.3 Liquid scintillators

Liquid scintillators used in large underground detectors must satisfy strict safety conditions, and in particular must have a high flash point. Among the commercial products that meet these requirements, we have tested one scintillator based on diisopropylnaphthalene: Quickszint 801A from Zinsser[4]; and two scintillators based on mineral oil: BC-517L from Bicron[5], and EJ-399-04 from Eljen[6]. In addition, we have investigated the properties of several new liquid scintillators potentially suited to our purposes. Four types of base have been considered: VM-1 vacuum oil from MNPZ[7], transformer oil (TO), vaseline oil (VO) and diesel (DS). All of these bases were subjected to a special purification procedure, which greatly increased their light-transmission properties. Five different scintillating dopants have been tested, at various concentrations: naphthalene (NAP), 2,5-diphenyloxasol (PPO), 1,4-bis-(5-phenylaxazolyl-2-yl)-benzene (POPOP), and 1,4-bis-(4-methyl-5-phenylaxazolyl-2-yl)-benzene (DMPOPOP).

Scintillator light yields and decay times have been measured following a procedure described elsewhere [12, 13]. Results obtained, both with the commercial LS and with the new LS, are summarised in Table 1. Measurements were performed with the LS exposed to air, and have an uncertainty of about ± 10 %. Quickszint 801A had a refractive index of about 1.6; the other LS considered all had refractive indices in the range 1.47−1.49.

The chemical compatibility of the LS with polycarbonate, and with the plastic WLS fibres, has been studied in four tests.

In the first test, polycarbonate cells and Y11 fibres were immersed in Quickszint 801A at a temperature of 60 °C. About 2 cm of fibre core were dissolved after three days, and damage to the polycarbonate was evident after five days. This means that, despite its high light output (Table 1), Quickszint 801A cannot be used for our application.

In the second test, a study was carried out of the effect of BC-517L doped with 0.7 % naphthalene on the fibre transmission properties. A fibre with a length of 6 m was immersed in the scintillator and kept at room temperature. Blue light was input at one end of the fibre, and the output at the other end was monitored with a photomultiplier

[4]Zinsser Analytic Ltd., Maidenhead, Berkshire, SL6 1AP, United Kingdom.
[5]Bicron, Newbury, OH 44065-9577 USA
[6]Eljen Technology, Sweetwater, TX 79556 USA
[7]MNPZ, 222 Prospekt Mira, Moscow, Russia.

Table 1: Light yields and decay times for bases and liquid scintillators. The light yield, $I_0$, is expressed as a percentage of the light yield of anthracene. The light decay (where measured) is described as a single exponential with decay time $\tau_1$, or as the sum of two exponentials, with decay times $\tau_1$, $\tau_2$ and relative intensities $A_1$, $A_2$.

| Base or scintillator | $I_0$ (%) | $\tau_1$ (ns) | $A_1$ | $\tau_2$ (ns) | $A_2$ |
|---|---|---|---|---|---|
| Quickszint 801A | 80 | – | – | – | – |
| BC-517L | 39 | 2.0 | 1 | – | – |
| EJ-399-04 | 53 | 3.5 | 1 | – | – |
| VM-1 (vacuum oil) | 1.3 | 3.3 | 0.64 | 91 | 0.36 |
| TO (transformer oil) | 1.0 | 45 | 1 | – | – |
| VO (vaseline oil) | 0.67 | 6.3 | 0.27 | 81 | 0.73 |
| DS (diesel) | 0.90 | 34 | 1 | – | – |
| VM-1 + 0.01 % DMPOPOP + 1 % PPO + 3 % NAP | 40 | 9.6 | 0.72 | 112 | 0.28 |
| VM-1 + 0.02 % POPOP + 1 % PPO + 3 % NAP | 35 | 6.3 | 0.59 | 49 | 0.41 |
| TO + 0.01 % DMPOPOP + 1 % PPO + 3 % NAP | 40 | 6.3 | 0.68 | 44 | 0.32 |
| VO + 0.01 % DMPOPOP + 1 % PPO + 4 % NAP | 35 | 8.9 | 0.73 | 71 | 0.27 |
| DS + 0.03 % DMPOPOP + 1 % PPO + 3 % NAP | 40 | 7.2 | 0.73 | 30 | 0.27 |

over a period of 35 days. Results, shown in Fig. 5, indicate no deterioration in the fibre transmission characteristics.

In the third test, WLS fibres with a length of 1 m were inserted into metal tubes filled with one of three scintillators: BC-517L doped with 0.7 % naphthalene; EJ-399-04; VM-1. The tubes were irradiated at room temperature using a $^{90}$Sr source, and the light output was monitored with a photomultiplier over a period of nearly 500 days. Results are shown in Fig. 6. Within the experimental uncertainties, no change in performance is observed during this period.

In the fourth test, short lengths of WLS fibre were placed in containers that were again filled with one of the scintillators BC-517L doped with 0.7 % naphthalene; EJ-399-04; VM-1. The containers were kept at a temperature of 60 °C, and the physical condition of the fibre segments was monitored over a period of 60 days. The chemical action during this high-temperature test was equivalent to that expected in more than nine years at room temperature. At the end of the test, the fibre segments placed in doped BC-517L or in VM-1 were still in good condition. In contrast, the fibre segments placed in EJ-399-04 had suffered severe erosion of the core material.

The new scintillators tested have a performance comparable with that of the commercial products, and have a lower cost. As the new scintillators had not been produced in the volume required ($\sim$ 200 l) at the time of the present tests, we used BC-517L doped with 0.7 % naphthalene. The addition of the naphthalene improved the light

output by $\sim 13$ % as compared with standard BC-517L. The emission spectrum of this doped LS is shown in Fig. 2.

### 2.4 Fibre readout

The testbeam setup was such that either a readout device or a mirror could be optically coupled to the fibres at each end of a module. In most of the tests performed, modules had a mirror placed at one end and were read at their other end using an optoelectronic chain (Fig. 7). This consisted of an electrostatically focused image intensifier followed by a gateable electron-bombarded CCD (EBCCD), both made by Geosphaera[8]. The image intensifier had an input window with a diameter of 40 mm, and introduced a magnification of 0.62. The device's multialkali photocathode had a quantum efficiency of 18−20 % at the wavelengths emitted by the WLS fibres (Fig. 4). The phosphor screen had a decay time of the order of 100 $\mu$s, and acted as an optical memory while waiting for the trigger decision. For particles crossing the modules close to the non-readout end, the mirror increased the light output by about 70 %.

The EBCCD [14] is essentially a zoomable image intensifier with a reversed, thinned CCD mounted in place of the phosphor screen. The voltage of the zoom electrode was set so as to demagnify the image by a factor of 1.4. The CCD consisted of $1024 \times 1024$ pixels of $13 \times 13$ $\mu$m$^2$.

With the magnification chosen, the image of a single fibre fitted in a square of $42 \times 42$ pixels. The image of the fibres from six modules used in the second testbeam study is shown in Fig. 8. The image shows the orderly arrangement of the fibres, and allows identification of fibres that are damaged. With optimal (honeycomb) packing, the maximum number of fibres that could be read by the optoelectronic chain was about 600.

A trigger was defined by a coincidence between plastic scintillators and Cerenkov counters, placed in the beam line. The CCD was cleared by continuous readout. When a trigger arrived, the clearing was interrupted and a 300 $\mu$s gate pulse was applied to the EBCCD, enabling image transmission. Image data were digitised and recorded using a Picasso PCI-LS frame grabber from Arvoo[9].

During the second testbeam study, readout was also performed using a hybrid photodiode (HPD) by DEP[10]. This read one side of a module, while the other side was read using the EBCCD chain described above. The HPD had a fibre-optic input window with a useful diameter of 18 mm. Electrons released at the photocathode were accelerated across a potential difference of 8−10 kV and detected by 61 hexagonal silicon pixels, each pixel reading a single WLS fibre. At the wavelengths emitted by the fibres, the quantum efficiency of the HPD photocathode was 12−14 %, significantly lower than for the first photocathode in the EBCCD chain (Fig. 4).

## 3 Testbeam results

Testbeam measurements have been performed with modules placed so as to have fibre lengths perpendicular to the beam line. For the tests of the modules simulating the OPERA setup, monitoring of the beam was achieved using two multi-wire proportional

[8] Geosphaera Research Centre, Moscow 117261, Russia.
[9] Arvoo Eng. BV, 3440 AK Woerden, The Netherlands.
[10] Delft Electronic Products BV, 9300 AB Roden, The Netherlands.

chambers and four scintillator counters. A straight-line extrapolation through hits in the wire chambers was used to estimate the coordinate, $U_{wire}$, along an axis perpendicular to the fibres, of particles arriving at the LS tracker modules. Taking into account multiple scattering in the counters, the uncertainty on $U_{wire}$, for a particle of energy $E$, was approximately 8 mm/$E$(GeV).

Basic detector performance characteristics have been evaluated by examining the response of individual modules to a minimum-ionizing particle (m.i.p.). Additional measurements, using a 1−4 GeV $e^-$ beam, and with lead in front of the tracker modules, have been made in order to understand the detector response to electromagnetic showers. This is interesting for neutrino experiments, where $\tau^- \rightarrow e^- \nu_\tau \overline{\nu}_e$ decays are to be identified.

Results reported below are with a mirror at the non-readout end of the fibres in the case of readout by the EBCCD chain, and without mirror for readout with the HPD.

## 3.1 Measurements for minimum-ionizing particles

The fibre light output for particles crossing the detector modules at different distances, $d$, from the fibre readout end have been evaluated by counting the numbers of photoelectrons, $N_{pe}$, emitted at the first photocathode in the readout system. For readout with the EBCCD chain, a threshold pulse height was set for the CCD pixels, to eliminate electronic noise. A photoelectron from the first photocathode was then detected as a cluster of above-threshold pixels, centred on a local maximum (a pixel with a larger pulse height than the eight surrounding pixels). With the threshold chosen, the number of pixels per cluster was typically 3. In Fig. 9 we show, as an example, the $N_{pe}$ distribution for $d$ = 4.3 m, a cell cross section of 0.9 × 1.1 cm$^2$, and polycarbonate doped with 20 % $TiO_2$. For readout with the HPD, the number of photoelectrons emitted at the photocathode was evaluated for each pixel from the recorded pulse height, after calibration using a low-intensity light source.

The effect of cell dimensions on fibre light output has been investigated using the EBCCD chain and the module with cells having the same 0.9 cm thickness (along the beam) but different widths: 1.1 cm, 2.2 cm, 3.3 cm. A smaller cell width is found to give a higher light output, as shown in Fig. 10. This decrease of light output with increasing cell width is well reproduced by a Monte-Carlo simulation. This simulation takes into account the cell geometry, the fibre position inside a cell, the light attenuation in the LS and the reflectivity of the cell walls. Results in the remainder of this section relate to the modules with cells of 0.9 × 1.1 cm$^2$.

The mean number of photoelectrons, $\overline{N}_{pe}$, varies as a function of the distance of the traversing particle from the fibre readout end. This variation was measured in the first testbeam study (polycarbonate doped with 8 % $TiO_2$, EBCCD chain) for fibres in different cells (Fig. 11a). Mean numbers of photoelectrons were also measured, in the second test beam study (polycarbonate doped with 20 % $TiO_2$, EBCCD chain), for two choices of $d$ (Fig. 11a). The increase as compared with the corresponding measurements in the first testbeam study is due to the improved reflectivity of the cell walls. Data for individual fibres have been fitted with an exponential, to estimate the light-attenuation length. The distribution of attenuation lengths for all fibres considered is shown in Fig. 11b. The attenuation lengths measured in different cells are between 6.8 m and 11.6 m, with a mean value of $\lambda_{av}$ = 9.4 m. All modules tested gave similar results, demonstrating the reproducibility of the module characteristics.

Measurements of light yield as a function of the distance $d$ have also been performed

for fibres read by the HPD. Results for eight cells are shown in Fig. 11c and Fig. 11d. In this case, the average light-attenuation length in the fibres is measured to be $\lambda_{av} = 6.4$ m.

When comparing results for the different readout systems, it should be recalled that a mirror, with 70 % reflectivity, was placed at the non-readout end for the EBCCD chain, but not for the HPD.

### 3.2 Measurements for showering particles

The detector response to showering particles has been investigated using 1−4 GeV $e^-$ directed onto a module at $d = 4.3$ m. The module was read by the EBCCD optoelectronic chain.

Measurements of shower intensity and spread have been made with 5.6 cm of lead in front of the module tested. The 10 radiation lengths of lead correspond to the material (lead plus emulsion) of a single brick in the setup of a typical neutrino experiment, such as OPERA [7].

Distributions of $N_{pe}$, representing shower intensity, are shown in Fig. 12 for showers generated by electrons of 2 GeV and 4 GeV. The ratio between the $\overline{N}_{pe}$ values of $79.5 \pm 2.3$ for 4 GeV $e^-$ and $38.1 \pm 1.3$ for 2 GeV $e^-$ is $2.1 \pm 0.1$. This is in satisfactory agreement with the ratio of 2.3 expected from a well-established electromagnetic-cascade model [15], reflecting the linear response of the detector and readout system.

Measurements of shower spread have been obtained by superimposing histograms of the number of photoelectrons per cell, centring on the maximum, for many events. The profile for a 4 GeV shower is compared in Fig. 13 with the analogous profile for a 4 GeV $e^-$ when no lead is in front of the tracker module. In the latter case, all incoming particles traverse the cell corresponding to the central bin, and the small number of photoelectrons seen on either side are essentially due to crosstalk.

The coordinate of shower origin along an axis perpendicular to the fibres in a module is estimated as the weighted mean, $U_{cell}$, of the coordinates of the affected cells. The weights are the cell light outputs, measured in photoelectrons. The precision of the coordinate estimated using the LS tracker is evaluated by comparing $U_{cell}$ with the coordinate, $U_{wire}$, obtained for the incoming particle using the wire chambers of the beam monitor. Distributions of $\Delta U = U_{wire} - U_{cell}$ for incoming $e^-$ of 1 GeV, 2 GeV and 4 GeV have been measured, with varying amounts of lead in front of the tracker modules. Examples for 4 GeV $e^-$, with 5.6 cm of lead present and with no lead, are shown in Fig. 14. The central part of each of the distributions measured is fitted by a Gaussian to determine the standard deviation, $\sigma_{\Delta U}$. The variation of $\sigma_{\Delta U}$ with $e^-$ energy and lead thickness is plotted in Fig. 15. The energy dependence of $\sigma_{\Delta U}$ when no lead is in front of the tracker is consistent with the multiple scattering in the beam counters. As expected, the precision in transverse shower position given by the tracker modules worsens as the material thickness increases and as the shower energy decreases. For a lead thickness of 10 radiation lengths, the position uncertainty is of the order of a few millimetres at 4 GeV and is 1.5−2.0 cm at 1 GeV.

## 4 Conclusions

Large electronic trackers for the detection of neutrino interactions in long-baseline experiments have been studied. Module prototypes have been assembled from polycarbonate panels having a surface area of $1 \times 6$ m$^2$ or $0.55 \times 6$ m$^2$. Panels were subdivided

into cells with a cross section of $\sim 1$ cm$^2$ and a length of 6 m. Each cell was filled with liquid scintillator and read using a WLS fibre. To increase the light captured by a fibre, and to reduce the optical crosstalk between neighbouring cells, the polycarbonate was doped with $TiO_2$. The maximum concentration of $TiO_2$ compatible with the panel extrusion process is 20 %, for which the crosstalk on each side of a cell was at the level of $\sim 3$ %. The effect of cell dimensions on light-collection efficiency has been investigated using cells having the same 0.9 cm thickness but different widths: 1.1 cm, 2.2 cm, 3.3 cm. Higher light output was obtained with smaller cell size.

New oil-based liquid scintillators have been investigated. These have a high flash point, compatible with their use in underground experiments, where strict safety requirements must be satisfied. The new scintillators have a low cost, and offer a light yield comparable to that of commercial scintillators, making them good candidates for large detectors. As the new scintillators are currently available only in small quantities, the polycarbonate panels used in testbeam studies were filled with BC-517L doped with 0.7 % naphthalene. Two readout systems have been tested: an optoelectronic chain, comprising an image intensifier and an EBCCD; and a hybrid photodiode. The average number of photoelectrons for minimum-ionizing particles crossing a detector module was, depending on crossing point, $6-12$ with the EBCCD readout and mirror at non-readout end; $4-10$ with the HPD readout and no mirror. The corresponding light-attenuation lengths in the fibres were $\sim 9.4$ m (EBCCD readout) and $\sim 6.4$ m (HPD readout).

The response of the detector to electromagnetic showers has been investigated using $1-4$ GeV electrons. A variable thickness of lead was placed in front of a panel read by the EBCCD chain. The total amount of light measured for electron showers of different energies agrees with that expected from a well-established electromagnetic-cascade model. Measurement of the shower profile transverse to the beam line allows the position of the incoming electrons to be determined with a precision of a few millimetres at an energy of 4 GeV, and with a precision of $1.5-2.0$ cm at 1 GeV.

In conclusion, the characteristics of trackers based on polycarbonate panels filled with liquid scintillator, and read using WLS fibres, are well matched to the requirements for large underground neutrino experiments. The EBCCD chain gives a higher number of photoelectrons than the HPD, because it has higher quantum efficiency for the light emitted by the WLS fibres. The HPD has the advantage that it is a self-triggering device, giving information on event timing, whereas the EBCCD needs to be gated by an external trigger signal.

# Acknowledgements

We would like to thank C. Coluzza (Università di Roma "La Sapienza") for measuring the reflectivity of the polycarbonate tubes. The Brussels group thanks the Institut Interuniversitaire des Sciences Nucléaires (Belgium) for financial support. This work was partly supported through the European Union's TMR Network Contract ERBFMRX-CT98-0196.

# References


[1] S. Hatakeyama et al., Phys. Rev. Lett. 81 (1998) 2016, and references therein.

[2] W. W. M. Allison et al., Phys. Lett. B 449 (1999) 137, and references therein.

[3] M. Ambrosio et al., Phys. Lett. B 434 (1998) 451.

[4] Y. Fukuda et al., Phys. Lett. B 467 (1999) 185, and references therein.

[5] S. H. Ahn et al., Phys. Lett. B 511 (2001) 178.

[6] E. Ables et al., FNAL proposal P-875: MINOS note NuMI-L-63 (1995); P. Adamson et al., MINOS TDR NuMI-L-337 (1998).

[7] M. Guler et al., OPERA Experimental Proposal, CERN/SPSC 2000-028; SPSC/P318; LNGS P25/2000 (2000).

[8] K. Kodama et al., Phys. Lett. B 504 (2001) 218.

[9] M. Doucet et al., Nucl. Instr. and Meth. A 453 (2000) 545.

[10] M. Doucet et al., Nucl. Instr. and Meth. A 459 (2001) 459.

[11] P. Border et al., Nucl. Instr. and Meth. A 463 (2001) 194.

[12] S. Buontempo et al., Nucl. Instr. and Meth. A 425 (1999) 492.

[13] G.I. Britvich et al., Nucl. Instr. and Meth. A 425 (1999) 498.

[14] S. Buontempo et al., Nucl. Instr. and Meth. A 413 (1998) 255.

[15] D.E. Groom et al. (Particle Data Group), Euro. Phys. J. C 15 (2000) 1.

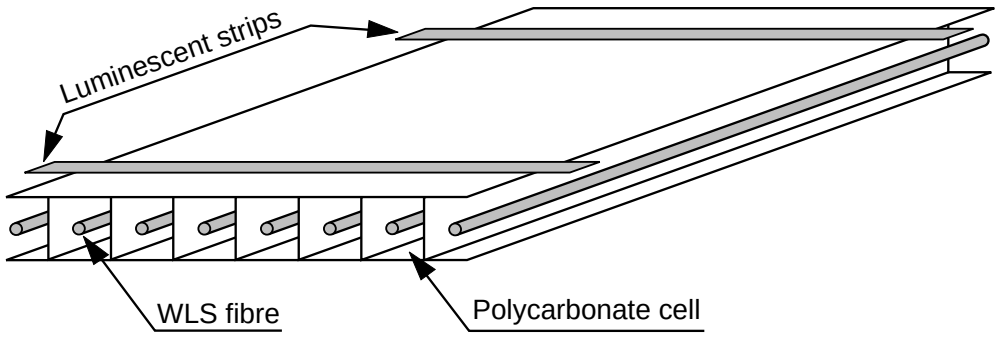


Figure 1: Schematic view of the polycarbonate cells and WLS fibres in a section of a detector module. Each cell has a cross-section of $0.9 \times 1.1$ cm$^2$ and a length of 6 m. The electro-luminescent strips are used for calibration.

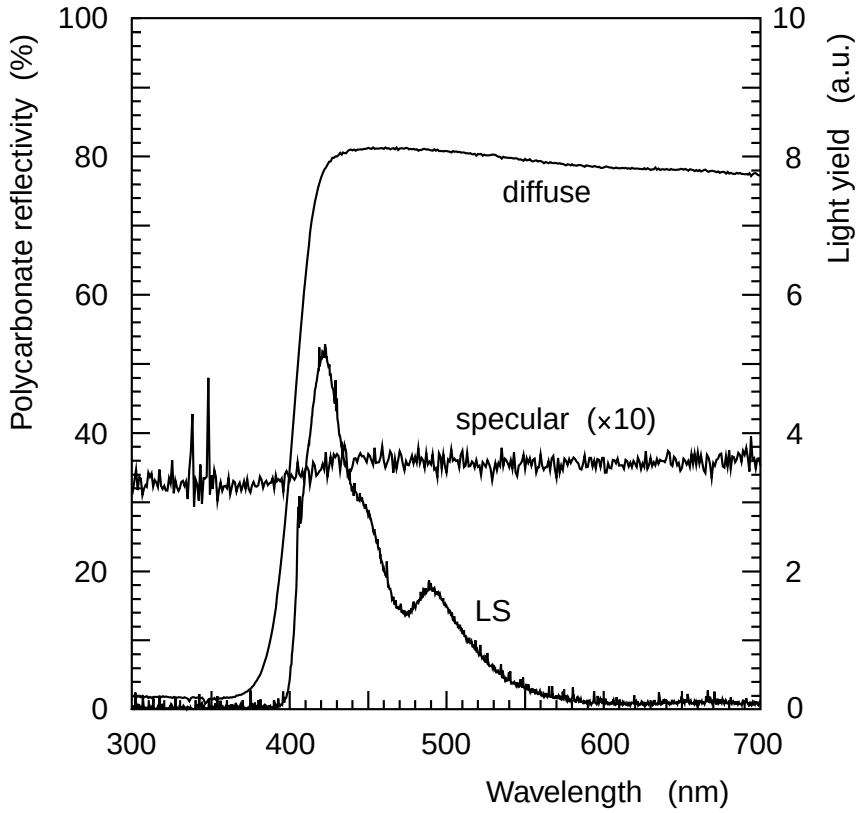


Figure 2: Reflectivity as a function of wavelength for polycarbonate doped with 20 % $TiO_2$, with specular and diffuse components shown separately (left scale). The emission spectrum for the liquid scintillator (LS) BC-517L doped with 0.7 % naphthalene is superimposed (right scale).

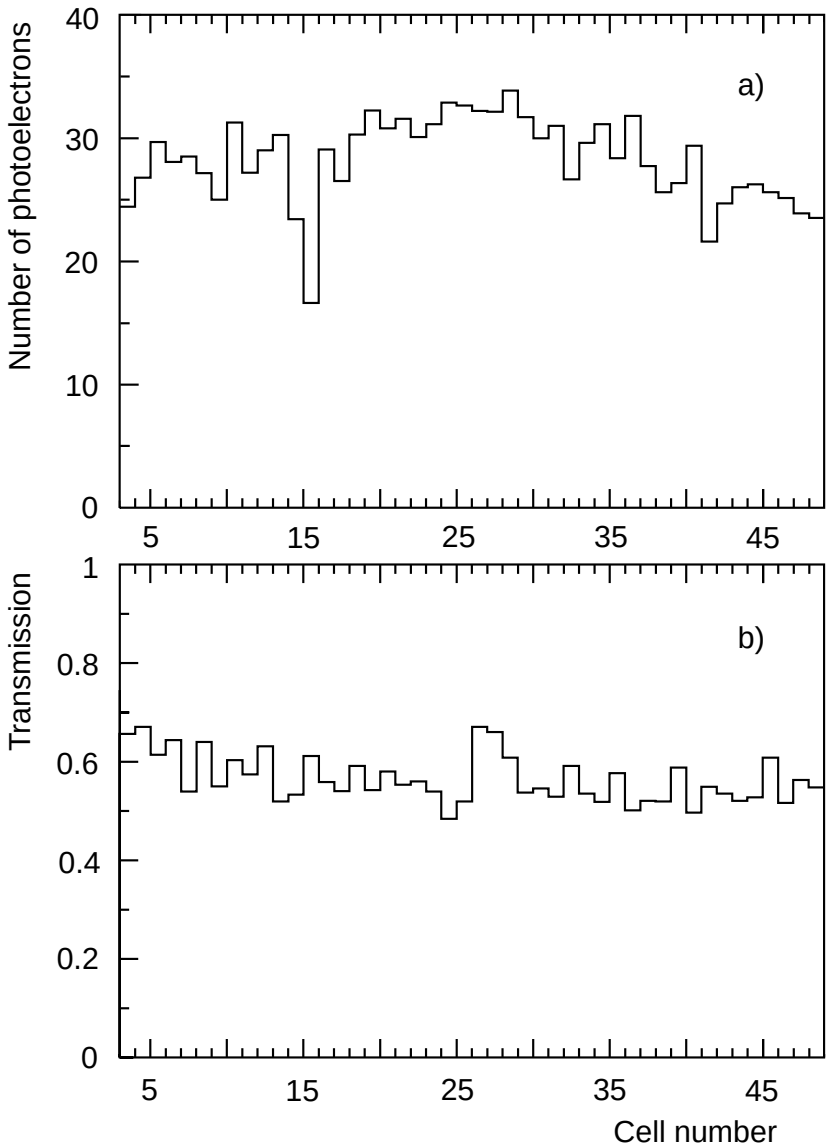


Figure 3: Measurements of: a) light recorded from fibres lit by the electro-luminescent strip nearer the readout end; b) ratio between the light from the fibres when the strip more distant from the readout end is pulsed and the light when the nearer strip is pulsed. A depression in correspondence to the 15th fibre is present in a) but not in b). This indicates that this fibre is damaged at a point outside the region between the two strips. Data for the two outermost cells on each side were not recorded for this measurement.

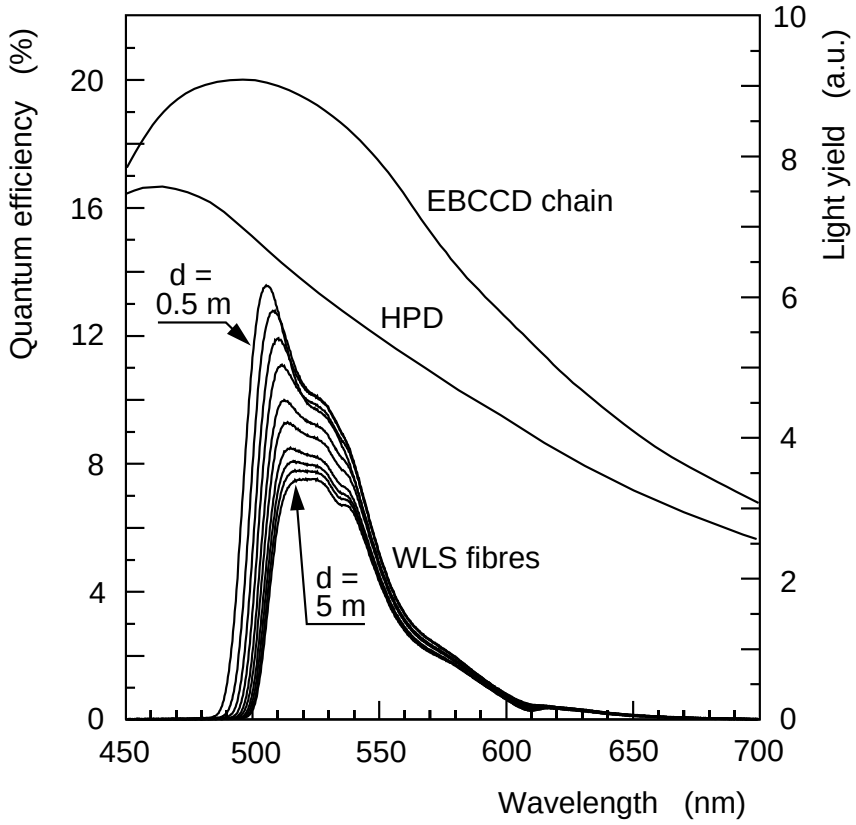


Figure 4: Upper curves (left scale): Quantum efficiency, as a function of wavelength, for the first photocathode of the two fibre-readout systems tested: EBCCD chain and HPD. Lower curves (right scale): Spectra for light emerging from the WLS fibres, for different values of the distance $d$ between emission point and fibre end. The ten curves are for values of $d$ from 0.5 m to 5 m, in steps of 0.5 m. Self-absorption causes the light to be more strongly attenuated at shorter wavelengths.

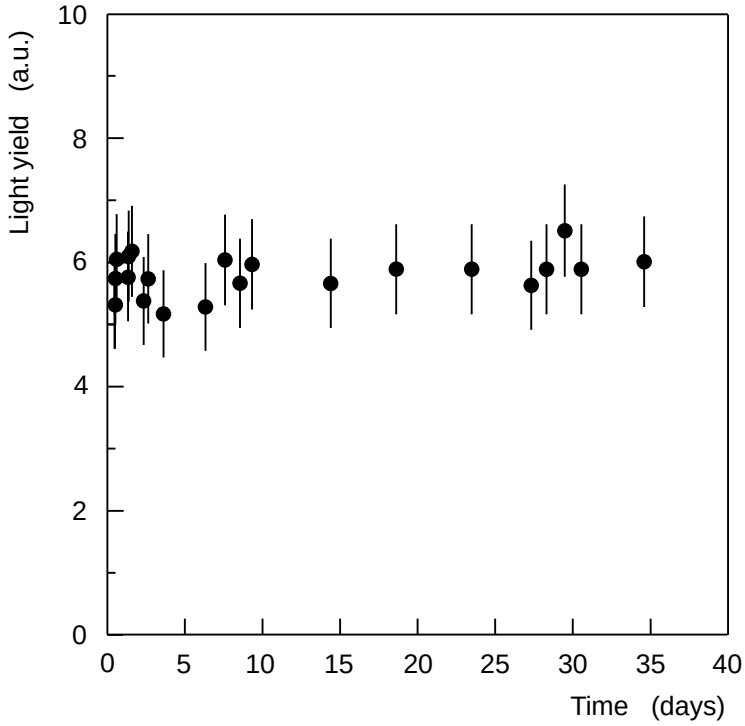


Figure 5: Light transmission in a 6 m WLS fibre immersed for 35 days in BC-517L liquid scintillator doped with 0.7 % naphthalene. No deterioration in the fibre characteristics is observed during the immersion.

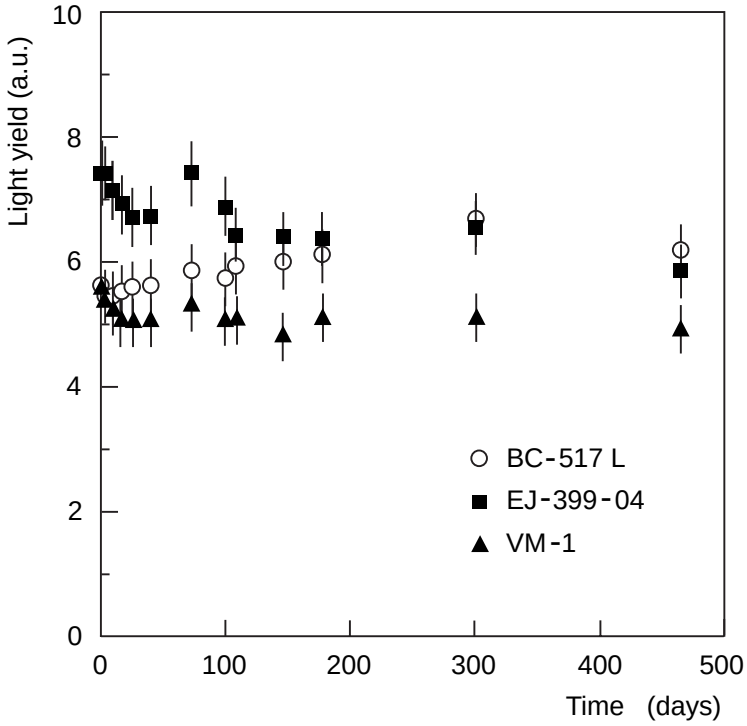


Figure 6: Long-term stability of a WLS fibre immersed in three liquid scintillators, and irradiated at room temperature using a $^{90}$Sr source.

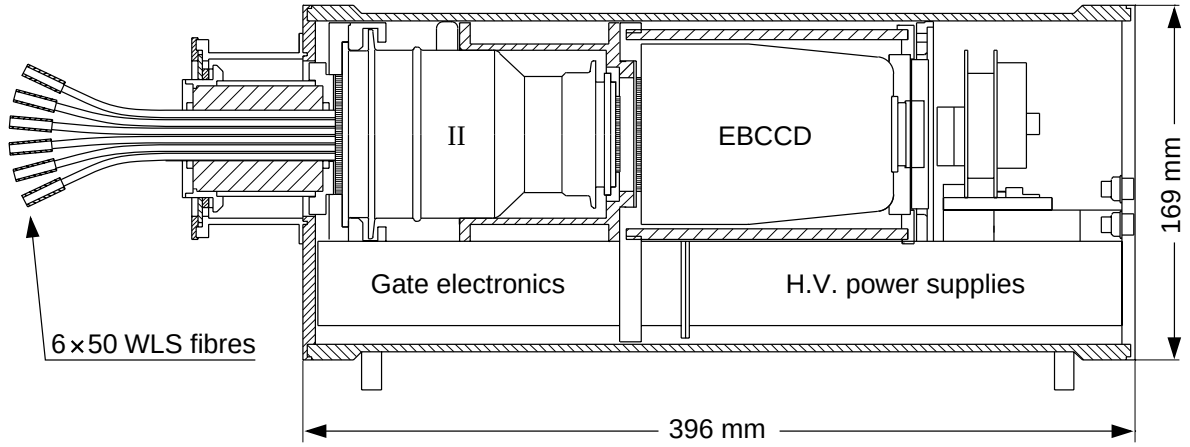


Figure 7: Optoelectronic chain used to read six detector modules. The chain comprises an image intensifier (II) and an electron-bombarded CCD (EBCCD).

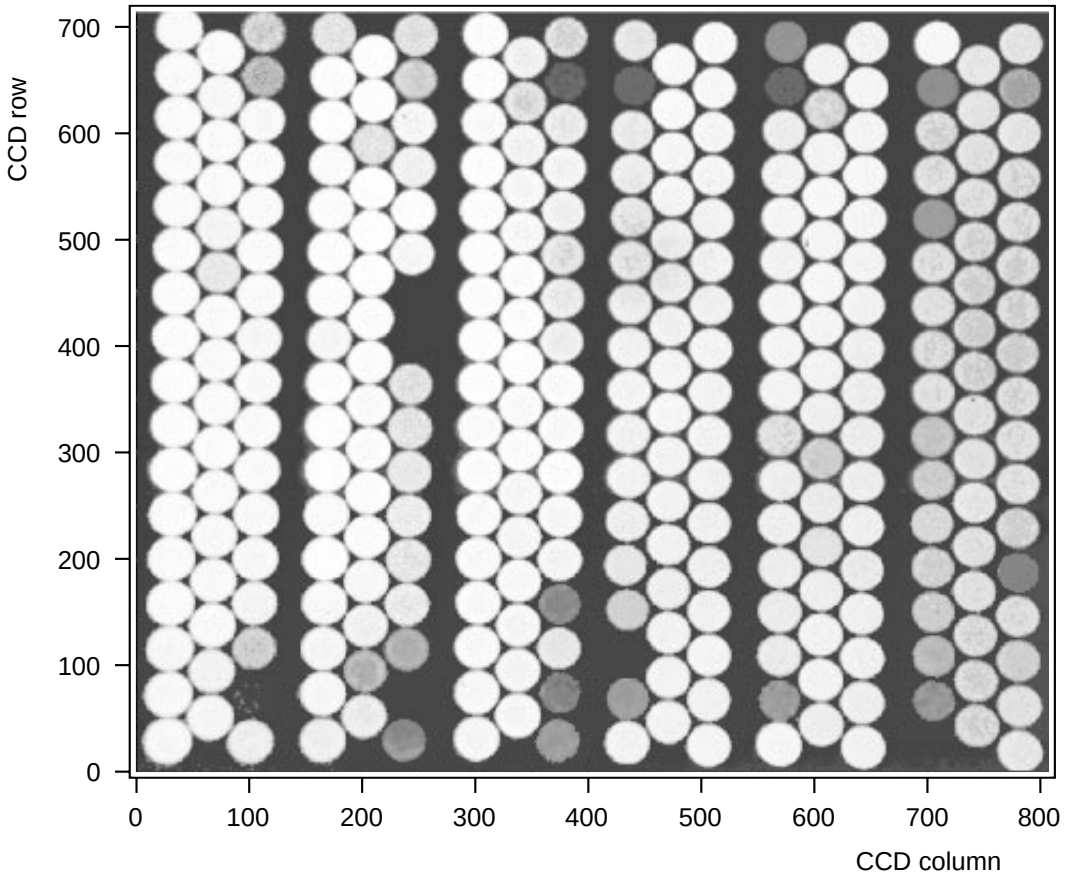


Figure 8: Image of fibres from six modules used in the second testbeam study. Light was input to the fibres using the electro-luminescent strips attached to each module, and the fibre outputs were recorded at the EBCCD. The 50 fibres contained in a single module were grouped into 3 columns for readout. Variations in the average light intensity per module reflect variations in the level of illumination. Fibres with a very low light output are damaged.

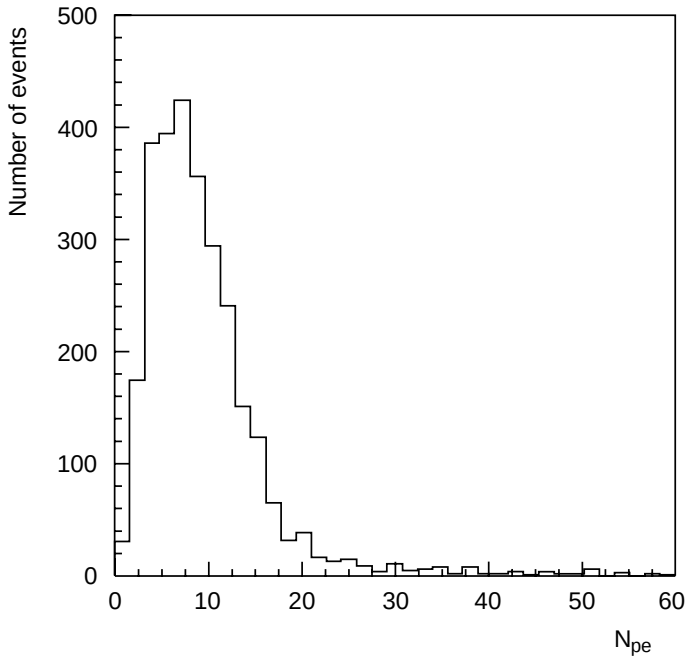


Figure 9: Distribution of number of photoelectrons, $N_{pe}$, emitted at first photocathode of EBCCD chain for minimum-ionizing particles crossing a module at a distance $d = 4.3$ m from the fibre readout ends.

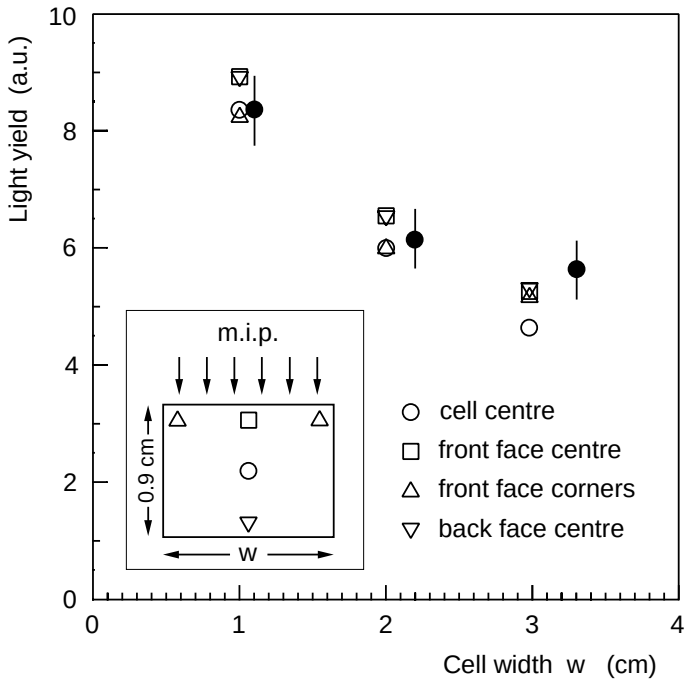


Figure 10: Relative light output of fibres as a function of cell width transverse to beam, as found experimentally (shaded circles) and as calculated with a Monte-Carlo simulation (unshaded symbols). The cell dimension along the beam direction was 0.9 cm. In the simulation, several possibilities for the fibre position within the cell have been considered (see insert), showing that the fibre location is not critical.

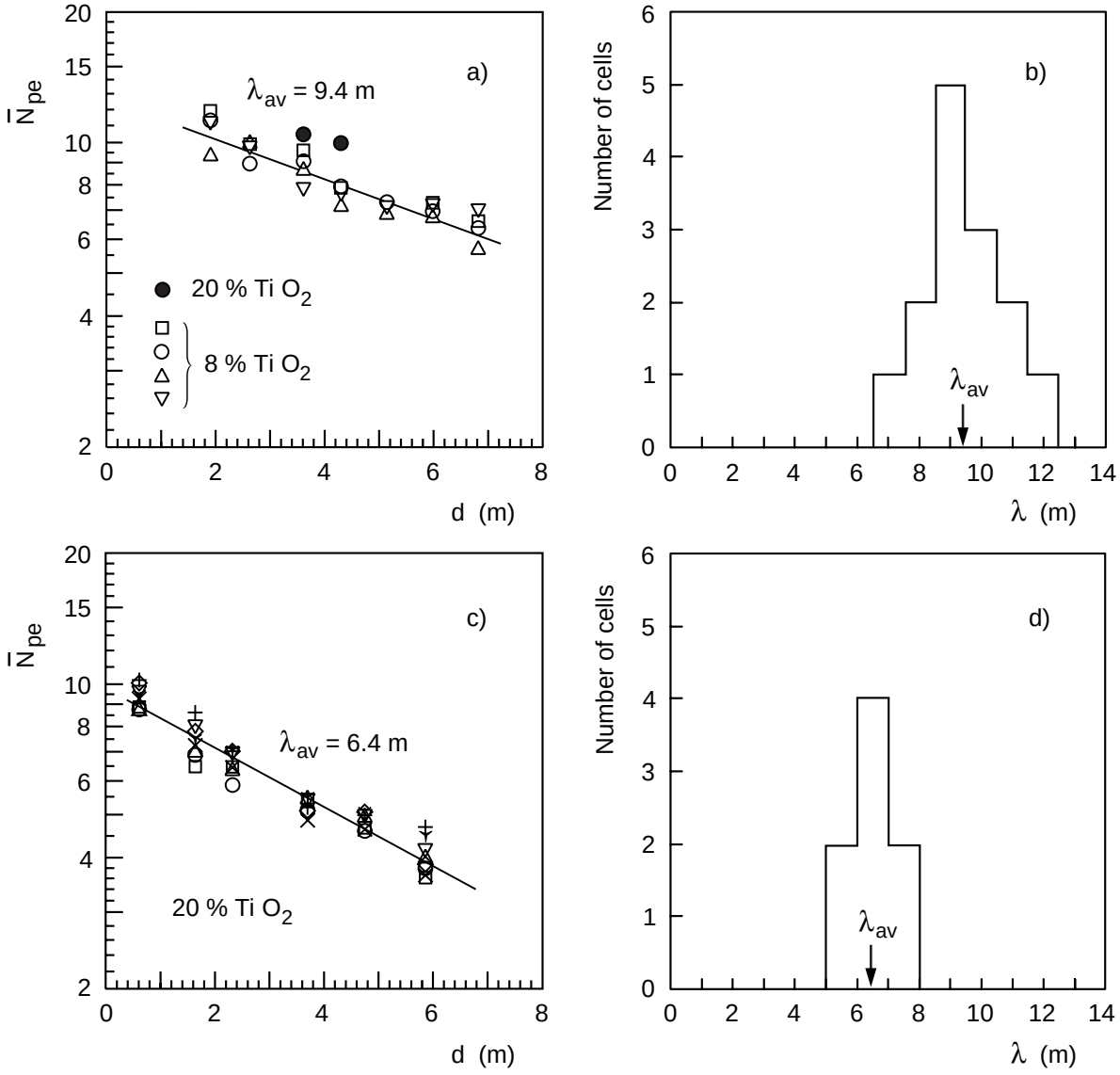


Figure 11: a) Average number of photoelectrons, $\overline{N}_{pe}$, emitted at first photocathode of EBCCD chain, as a function of particle distance, $d$, from the fibre readout ends. A mirror was positioned at the non-readout end. Measurements are shown for different cells, doped with 8 % or 20 % $TiO_2$ as indicated. The higher $TiO_2$ concentration gives a higher light yield. The curve shows the light-attenuation length ($\lambda_{av}$) in the fibres, averaged over different cells. b) Distribution of attenuation lengths with the EBCCD chain, for many cells. Results shown in c) and d) are as in a) and b), but were obtained using the HPD readout. These measurements were for polycarbonate doped with 20 % $TiO_2$, and with no mirror at the non-readout end of the fibres. The length of the fibres between the modules and the readout system was 1.5 m for the EBCCD chain and 0.5 m for the HPD.

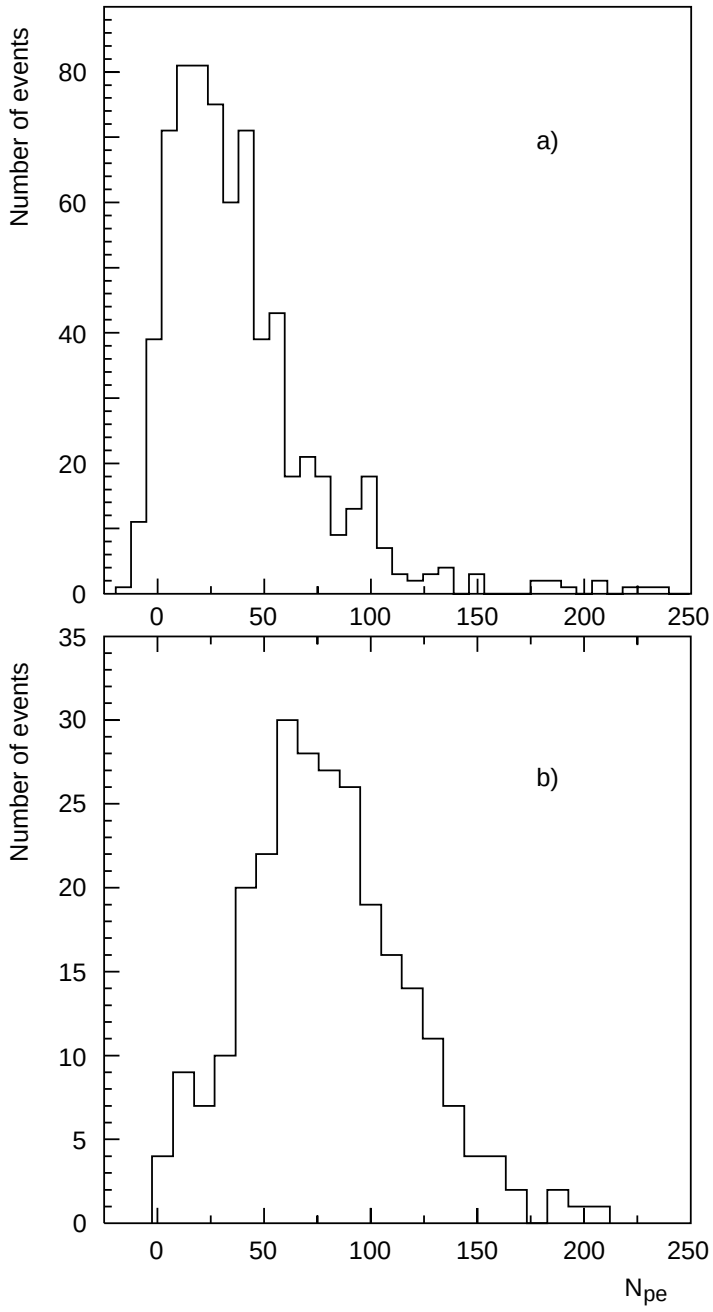


Figure 12: Distributions of numbers of photoelectrons, $N_{pe}$, emitted at first photocathode of EBCCD chain, for showers generated in 5.6 cm of lead by: a) 2 GeV $e^-$ and b) 4 GeV $e^-$. The line of flight of the incoming electrons crosses the module at a distance $d = 4.3$ m from the fibre readout ends. For each fired cell the average background per cell has been subtracted, resulting in negative values of $N_{pe}$ in a small fraction of cases.

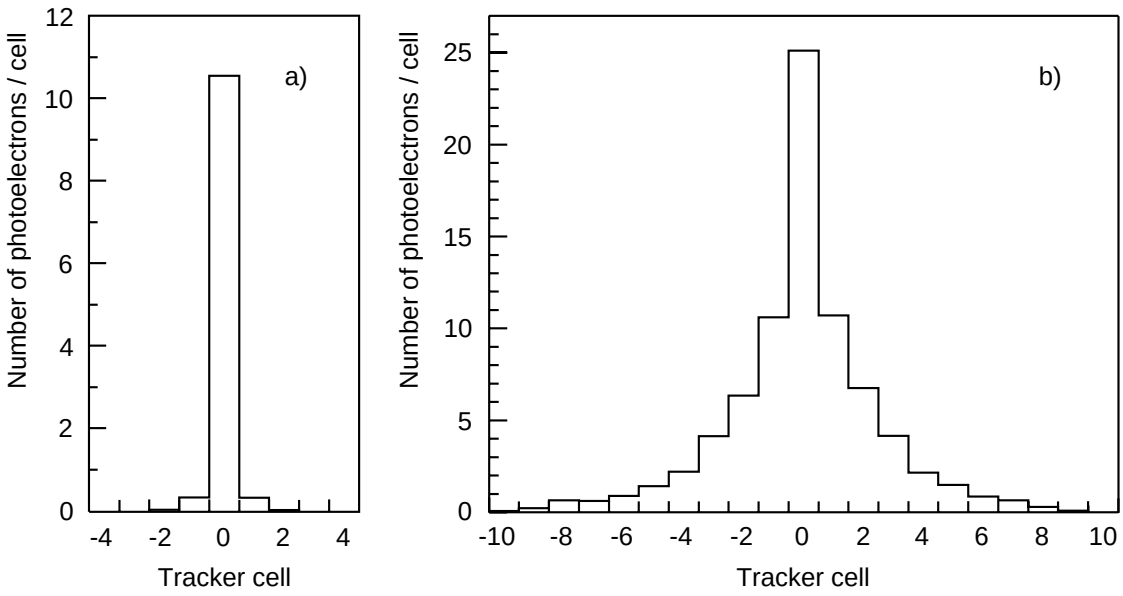


Figure 13: Intensity profiles, averaged over many events, for incoming $e^-$ of 4 GeV: a) with no lead present; b) with 5.6 cm of lead in front of tracker.

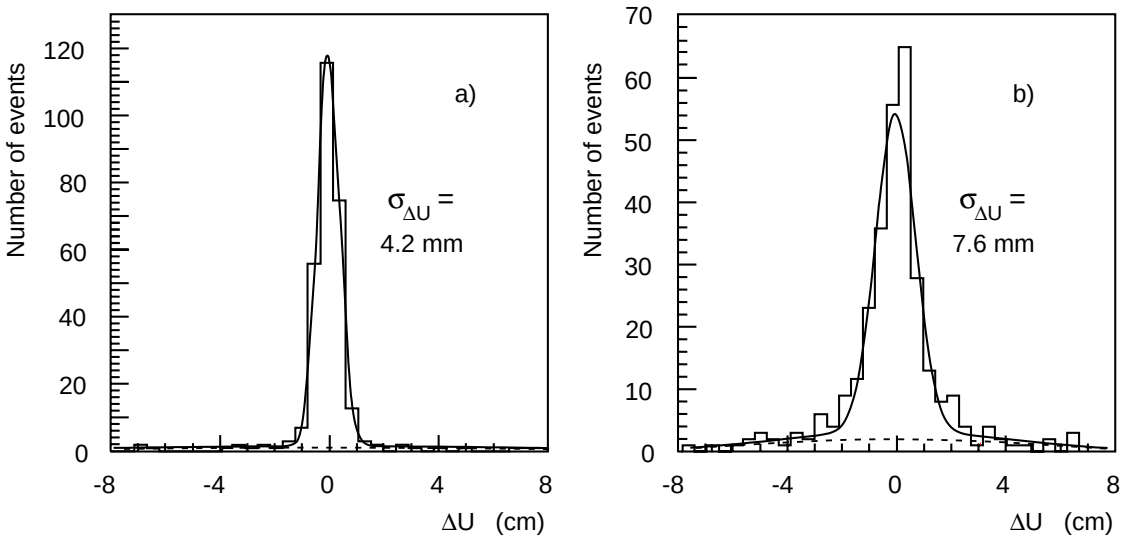


Figure 14: Distribution of difference, $\Delta U$, between particle position given by wire chambers and shower position given by LS tracker module, for incoming $e^-$ of 4 GeV: a) with no lead present; b) with 5.6 cm of lead in front of tracker. Each distribution is fitted by a Gaussian, of standard deviation $\sigma_{\Delta U}$, superimposed on a broad background.

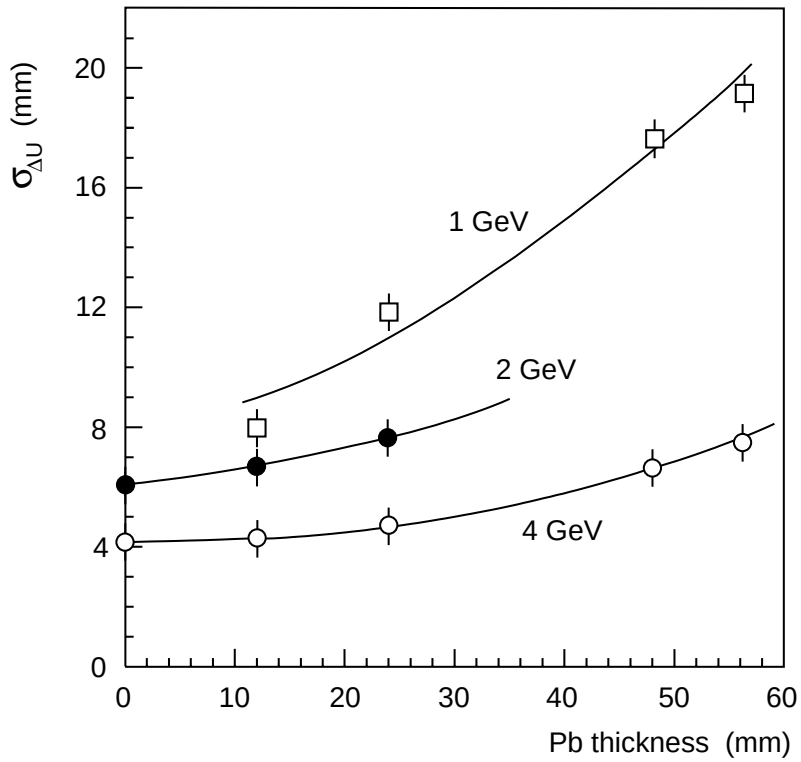


Figure 15: Variation with lead thickness and $e^-$ energy of the standard deviation, $\sigma_{\Delta U}$, characterising the distribution of the difference between particle position given by wire chambers and shower position given by LS tracker module. Curves are drawn to guide the eye.